Growth and decay of hcp-like Cu hut-shaped structures on W(100)

Tjeerd R. J. Bollmann,[1,2] Raoul van Gastel,[1] Herbert Wormeester,[1] Harold J. W. Zandvliet,[1] and Bene Poelsema[1]

[1]*Physics of Interfaces and Nanomaterials, MESA+ Institute for Nanotechnology, University of Twente, P.O. Box 217, NL-7500AE Enschede, The Netherlands*

[2]*Fachbereich Physik, Universität Osnabrück, Barbarastraße 7, 49076 Osnabrück, Germany*

(Received 12 July 2011; revised manuscript received 21 February 2012; published 14 March 2012)

We have studied both the morphology and structure of thin Cu deposits on W(100) during growth and desorption, using low-energy electron microscopy (LEEM) and selective area low-energy electron diffraction (μLEED). During growth at 674 K hut-shaped Cu crystallites with steep facets ($>54^\circ$) coexist with a pseudomorphic Cu monolayer. The μLEED data suggest that these crystallites predominantly have a hcp structure with a high density of stacking faults and the $(11\bar{2}0)$ plane parallel to W(100). The boundaries run along the $[\bar{1}50]$ azimuth on W(100), which is explained by cancellation of shear stress exerted by Cu on the W(100) surface. Upon slow heating, Cu desorbs and the pseudomorphic wetting layer is transformed into coexisting surface alloy patches, with respectively, a Cu-rich $p(2 \times 2)$ and $p(2 \times 1)$ structure at 815 K. At about 950 K the islands are fully desorbed, leaving $p(2 \times 1)$ footprints behind. The $p(2 \times 2)$ patches disappear at about 1020 K, resulting in a homogeneous $p(2 \times 1)$ surface. Upon continued Cu desorption this surface transforms into small $c(2 \times 2)$ domains until all Cu has been desorbed at 1150 K.

DOI: 10.1103/PhysRevB.85.125417 PACS number(s): 68.55.−a, 68.37.Nq

I. INTRODUCTION

In thin-film growth, misfit-related stress between substrate and adsorbate together with the combined interfacial free energies govern the characteristic Stranski-Krastanov- or Volmer-Weber-type growth modes. Strong film-substrate interaction in combination with a large misfit will lead to accumulation of misfit-induced strain energy. The system usually responds by growing in a Stranski-Krastanov mode with relatively strain-free three-dimensional (3D) deposits. Examples are the (hut-shaped) clusters with specific facet crystallography and alignment with respect to the substrate, e.g., Ge on the Si(001) substrate which results in clusters that consist of four-sided pyramids with (four equivalent) facets.[1] With increasing distance to the interface, stress can be relieved efficiently.[2]

For adsorbates having different crystal structures that energetically slightly deviate from their equilibrium crystal structure, the growth can be even more complicated. Noble metals like Cu, with its equilibrium fcc structure, can be grown in its near equilibrium hcp or bcc structure,[3] depending on the substrate properties. It has been shown that on bcc (100) substrates, coexisting hcp and bcc structures, or solely hcp structures can be formed, depending on the ratio of the atomic radii of substrate and adsorbate and its bonding to the substrate.[4,5] With their ratio near one, e.g., Pd (Ref. 4) and Co (Ref. 6) show growth of coexisting hcp and bcc structures on W(100). For Cu on W(100), this ratio is slightly lower, resulting in hcp$(11\bar{2}0)$ structures for coverages over 2.5 ML.[7]

The growth of a few layers of Cu on W(100) has been studied in detail.[8–10] For submonolayer coverages a number of ordered surface structures are found to be in dynamic equilibrium at 800 K. These correspond to areas of pseudomorphic Cu, as well as of surface alloys with a $p(2 \times 1)$, $p(2 \times 2)$, and $c(2 \times 2)$ structure.[8,9] Having a smaller atomic radius, the Cu atoms increase the tensile surface stress of the surface alloys.[11] Studies on the growth of hcp structures, as well as their morphology at temperatures over 500 K, are rather limited.[4,7]

Here, we present a study on the growth, decay, and interrelationship of Cu structures grown on W(100) at temperatures ranging from 674 to 1150 K. By using *in situ* low-energy electron microscopy (LEEM) and selective low-energy electron diffraction (μLEED) we are able to probe the properties and ordering of both the first Cu layer as well as the growth of 3D islands.

This paper is organized as follows. We describe the experimental conditions in Sec. II. In Sec. III, we describe the formation of the first Cu layer along with the morphology of the Cu islands that form. In Sec. IV we discuss the structure of the islands, followed in Sec. V by their growth kinetics. The decay of the Cu islands at elevated temperatures is described in Sec. VI, and the structural changes of the wetting layer at these temperatures in Sec. VII. We summarize our conclusions in Sec. VIII.

II. EXPERIMENT

The experiments were performed in an Elmitec LEEM III instrument with a lateral resolution of 7 nm. A W(100) single crystal was cleaned by successive flashing in a background of oxygen, monitored by thermal desorption spectroscopy (TDS). Special care has been taken concerning the cleaning by using two-step flashing as described elsewhere.[12] The procedure was completed by sputtering cycles of 1 keV Ar^+ bombardment at room temperature followed by flash annealing. During cleaning, carbon contamination was observed, with a characteristic $c(2 \times 2)$ and $p(5 \times 1)$ LEED pattern.[13] The cleanliness of the sample was verified by Auger electron spectroscopy (AES) and LEEM. Copper was deposited from a Knudsen cell. The μLEED patterns have been obtained using a 1.4 μm aperture.

III. MORPHOLOGY

We monitor the growth of Cu using LEED at a temperature of 674 K. Shortly after deposition has started, $c(2 \times 2)$ LEED spots appear. This structure can be a simple adlayer, as

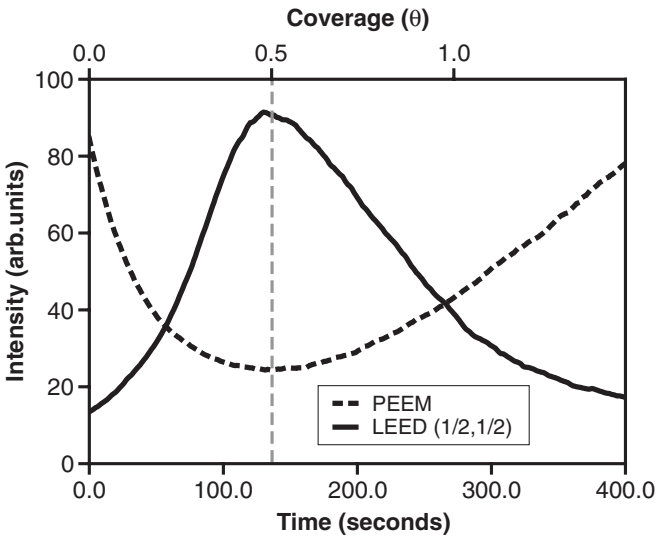

FIG. 1. Intensity of the $c(2 \times 2)$ μLEED spot (solid line) measured at 31.0 eV at a temperature of 674 K. The integrated PEEM intensity (dashed line) measured at a temperature of 674 K, shows a minimum at $\theta = 0.5$ ML.

well as a surface alloy having identical coverage.[8–10] Using the maximum intensity for the $(\frac{1}{2},\frac{1}{2})$ diffraction spots, a precise *in situ* calibration of the coverage can be made (see Fig. 1). For the $c(2 \times 2)$ structure $\theta = 0.5$ ML, where $\theta = 1$ ML corresponds to 1 Cu atom per W(100) surface atom. The measured deposition rate is 3.7×10^{-3} ML/s. The corresponding threshold photoemission electron microscopy (PEEM) intensity is a measure for the change in work function during deposition. The minimum in PEEM intensity as shown in Fig. 1, corresponds to a maximum in the work function. Following Attard and King[9] who claim a coincidence between a maximum in the work function and a simple $c(2 \times 2)$ adlayer, we assign the observed structure as being characteristic for an adlayer. Note that Attard and King found a $c(2 \times 2)$ alloy when the substrate temperature surpasses 800 K.

Completion of the first monolayer of Cu results in a pseudomorphic wetting layer, as is verified by LEED. The nucleation of islands is slightly lagging behind and only observed after deposition of about 1.35 ML. Note that, for small island sizes below $\theta = 1.5$ ML, the island sizes are hard to detect due to their small size and the finite lateral resolution of our instrument. The total fractional area of the islands only slowly extends to about 8% at a coverage of $\theta = 38.2$ ML (see Fig. 2). Therefore, we conclude that the growth of these islands has a strong 3D character, which we attribute to misfit-related stress. The island nucleation is delayed and it requires about 35% of a monolayer to initiate the growth of the 3D structures. A similar supersaturation has been observed for the nucleation of nanocrystals in Al(110) homoepitaxy.[14] The absence of any clear change of slope in the PEEM intensity near the monolayer coverage supports the continuous buildup of a diluted, supersaturated phase on top of the Cu wetting layer.

Literature shows some discussion on the wetting layer: the pseudomorphic growth is reported up to a coverage of 2 ML, after which hcp-like island growth is observed.[7] The fractional

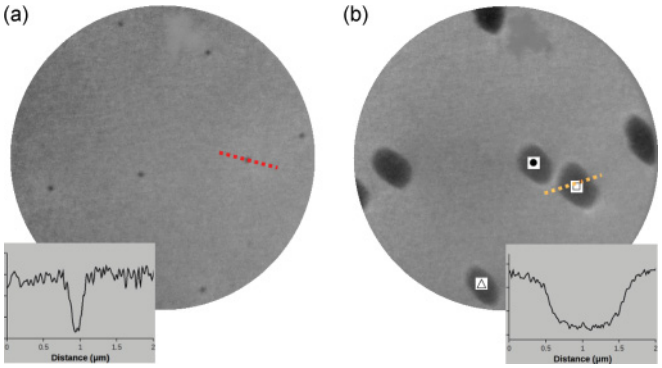

FIG. 2. (Color online) (a) and (b) LEEM images of Cu islands (dark) on a Cu wetting layer at a coverage of $\theta = 1.5$ ML (a) and $\theta = 38.2$ ML (b). The fractional area of Cu islands is small, 0.1% for (a) and 7.9% for (b), revealing strong 3D growth. Both images have a field of view (FoV) of 10 μm, electron energy 8.0 eV, and $T = 673$ K. The markers •, △, and □ refer to the islands, which are analyzed further in Fig. 5. Insets show line profiles as marked by the dotted lines.

area of the islands below $\theta = 2$ ML is, however, well below the sensitivity of reflection high-energy electron diffraction (RHEED). Our I/V-LEEM measurements show no indication for a double $p(1 \times 1)$ Cu layer. Apparently, the $p(1 \times 1)$ layer is only energetically favored up to the first layer, which is strongly bound to the substrate.

IV. Cu hcp-LIKE HUT-SHAPED STRUCTURES

μLEED with a 1.4 μm aperture was used for the structural characterization of the Cu islands shown in Fig. 2. For island areas only slightly smaller than the size of the used aperture, the μLEED pattern shown in Fig. 3(a) is observed. The spots originating from the W(100) substrate and thus the $p(1 \times 1)$ Cu layer are indicated by dashed circles. In addition, the pattern shows a number of additional intense spots marked by arrows, which at first sight do not correspond to a distinct pattern. This implies that no clearly developed two-dimensional order is

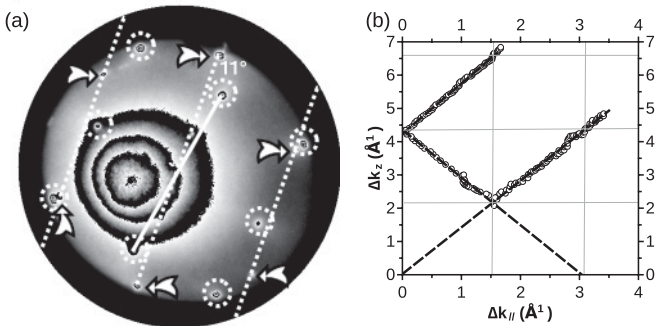

FIG. 3. (a) μLEED pattern of a Cu island measured at 32.5 eV. The LEED spots for W(100), and thus the pseudomorphic layer, are marked by dashed circles. The arrows mark the (6) facet spots, which move along the dashed lines upon varying the electron energy. The Cu island structure is azimuthally rotated by 11°. (b) A plot of the facet spot positions in reciprocal space. From the slope of these straight lines we obtain facet angles of 54°±3°. The intensity feature next to and left of the specular spot is caused by secondary electrons.

TABLE I. The misfit between the W(100) substrate and Cu films with various potential crystal structures along the indicated azimuth directions. The misfit m is defined as $m = a_{Cu}/a_W - 1$. The last column refers to the bulk interlayer distance (h).

Lattice misfit (m) for Cu films on W(100)					
	W(100); $\langle 100\rangle_\parallel$	m(%)	W(100); $[1\bar{1}0]_\parallel$	m(%)	h (Å)
Cu fcc	Cu(100); [110]	−19.3			1.81
	Cu(110); [100]	14.2	Cu(110); [100]	−19.2	1.28
	Cu(110); [110]	−19.3	Cu(110); [110]	−42.9	1.28
Cu bcc	Cu(001); [100]	−9.2			1.42
Cu hcp			Cu(11$\bar{2}$0); [0001]	−6.9	1.28
			Cu(11$\bar{2}$0); [1$\bar{1}$00]	−1.2	1.28

present on top of the Cu islands. Measuring the I/V-μLEED curve on a Cu island reveals that the additional spots move along the dashed lines in Fig. 3(a). Therefore, they represent facet spots arising from strong 3D growth. It is remarkable that the travel of these intense spots does not coincide with a low index direction on W(100). Its actual azimuthal direction makes an angle of about 11° with the close-packed orientation. The rate of motion as a function of electron energy reveals that steep facets are present on the Cu crystallites.[15] A plot of the positions of the diffraction spots in reciprocal space, i.e., in the ($\Delta k_\parallel$,Δk_z) plane, confirms this: the spot positions follow straight lines as is shown in Fig. 3(b). From the slopes of these lines we measure facet angles of 54°± 3°. The variation of the spot positions in the ($\Delta k_\parallel$,Δk_z) plane, also provides information on the perpendicular and in-plane periodicities. For the periodicity along the normal (Δk_z) we obtain 4.42 Å^{-1}, which corresponds to an interlayer spacing of 1.42 ± 0.08 Å. The periodicity of 1.55 Å^{-1}, found for the in-plane direction ($\Delta k_\parallel$) in Fig. 3(b), corresponds to a real-space periodicity of 4.05 ± 0.12 Å.

Table I summarizes the lattice misfit, defined as the ratio of the lattice parameters along the indicated azimuth minus 1, along the indicated azimuth directions. The results are shown for three different lattice structures: face-centered cubic (fcc), body-centered cubic (bcc), and hexagonally close packed (hcp). We make the assumption that the hcp structure has the density of the bulk fcc crystal. For bcc Cu we use the lattice constant of 2.86 Å available from literature.[16–18]

From the measured values we conclude that the misfits for the fcc Cu films are substantial, which leaves Cu bcc and hcp as candidates. From the clearly lesser misfit values for hcp we find Cu hcp as the most probable film structure in agreement with the results reported in Ref. 7. Indeed these authors concluded from their RHEED measurements, that in the Cu deposits, the hcp(11$\bar{2}$0) planes run parallel to the W(100) surface. The [1$\bar{1}$00] base vector of the almost square unit cell of the hcp(11$\bar{2}$0) planes fits perfectly along the [110] azimuth of W(100) with a misfit of only −1.2%. The perpendicular [0001] base vector has a misfit of −6.9% along the [1$\bar{1}$0] azimuth of W(100). It is also known from experiments that the close-packed facets are easy glide planes giving rise to twinning in fcc crystals. For Cu/W(100), a high density of faults in the stacking order perpendicular to the close-packed planes has been observed previously.[19]

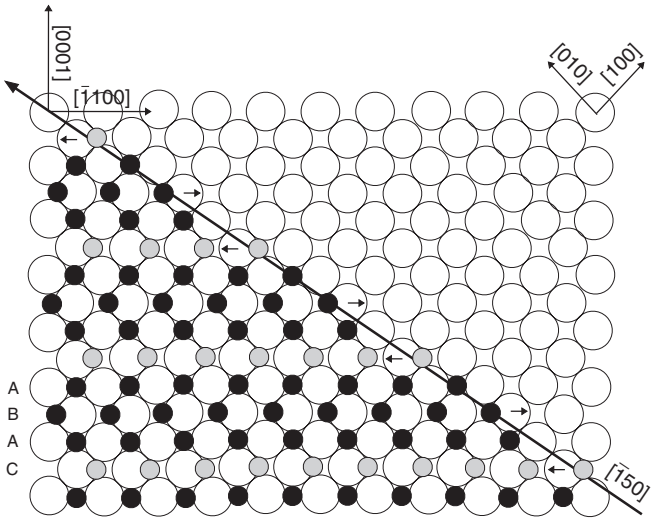

FIG. 4. Cartoon of the first layer of Cu atoms in the Cu crystallites (small circles) on the W(100) surface (large open circles). The pseudomorphic wetting layer, not shown for clarity, would consist of Cu atoms in fourfold hollow sites on the right-hand side of the black line along the W(100)-[$\bar{1}$50] azimuth. The latter shows the boundary between the crystallite and the wetting layer and makes an angle of 11.3° with the W(100)-[010] azimuth. The Cu atoms are drawn with the hcp crystal (11$\bar{2}$0) plane as a base. The gray circles represent a fault in the perfect AB-stacking sequence, shown by black circles. The cartoon shows an $(ABAC)_n$ stacking of the close-packed layers. The arrows indicate the direction of the exerted stress on the outermost W(100) layer by the Cu directly above. The [$\bar{1}$50] azimuth warrants a complete cancellation of the shear stress, indicated by arrows, along the W(100)-[1$\bar{1}$0] azimuth. We emphasize that the separation between the stacking faults is less regular than sketched here, while maintaining the average value.

First, we consider the interlayer distance between the Cu planes parallel to W(100). The measured value could hint at fcc Cu(011), bcc Cu(001), or hcp Cu(11$\bar{2}$0). Since we do not see clear indications for either fcc or bcc Cu in terms of a low misfit registry with respect to W(100)-$c(2\times 2)$, we resort to the hcp structure. The corresponding interlayer distance would be 1.28 Å, i.e., close to the measured value of 1.42 ± 0.06 Å. A peculiarity is the fact that the contact lines of the facets with the substrate are not parallel to the ⟨100⟩ directions of W(100), but rather intersect W(100) at an angle of about 11° with the ⟨100⟩ azimuth [see also Fig. 3(a)]. This finding can be rationalized by the fact that the square (11$\bar{2}$0) unit cell contains two atoms: one in the fourfold hollow site on W(100) and one on the center line along the W(100)-⟨110⟩ azimuth, situated at either $\frac{1}{3}$ or $\frac{2}{3}$ of the unit-cell boundary (see Fig. 4). This will lead to shear stress along ⟨100⟩ exerted by Cu on the W(100) surface. This stress can be significantly reduced if we allow for stacking faults. For the ideal case of an $(ABAC)_n$ stacking the shear stresses are canceled and we arrive at a strong candidate for a boundary between Cu and W along the [$\bar{1}$50] azimuth (see Fig. 4). It makes an angle of 11.3° with [010] on W(100), in agreement with the experimental observation in Fig. 3(a). Also, the steep facets can be easily realized: from the hcp (11$\bar{2}$0) structure and the 10% expanded interlayer distance, we obtain a facet angle of about 54°, in agreement with the experimental observation. This leads to quite smooth facets,

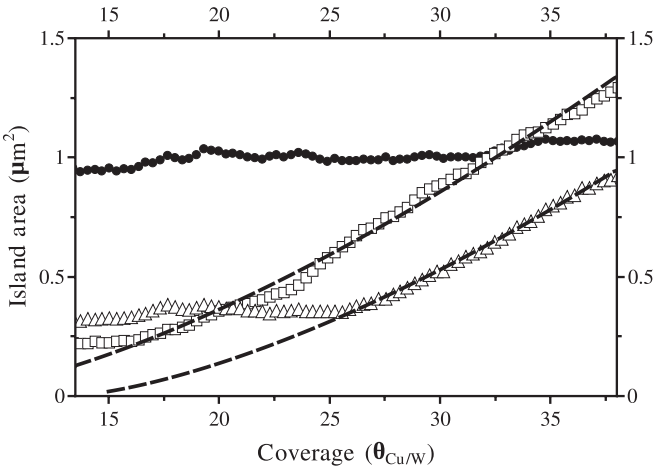

FIG. 5. Measured island area for increasing coverage for the islands (within the FoV during a slight thermal drift) labeled with •, △, and □, according to Fig. 2. The dashed lines show the best fit to $f \times a^p$, with $p = \frac{3}{2}$. It is not clear why the island denoted with black dots does not grow far beyond a linear scale of 1 μm^2. One may speculate that the accumulated stress hinders its further expansion.

and also explains the absence of a regular diffraction pattern since no extended areas with $(11\bar{2}0)$ orientation are expected on top of the hut-shaped Cu crystallites.

In addition, we mention that the average separation of the atoms along the $[\bar{1}50]$ azimuth, and therefore the periodicity, is 4.03 Å, i.e., very close to the experimental result of 4.05 Å. The compression of the Cu along the W(100)-[110] direction may also still lead to grains which are oriented in the [001] direction. The grain boundaries are probably light and their appearance, in line with previous reports,[19] would explain why the Cu islands are quite compact.

V. GROWTH DYNAMICS

As can be seen from Fig. 2, the hcp-like Cu island area only slowly increases during deposition. After the deposition of $\theta \approx 45$ ML the hcp-like Cu islands have a fractional coverage of 9.1%, resulting in an *average* island height of about 700 Å. We measured the area of the three marked islands of Fig. 2(b) as a function of global coverage, as is shown in the semilogarithmic plot in Fig. 5. We can study the growth dynamics where the available material for the hut structure is $\alpha(\theta - \theta_0)$, where α is the number of atoms that has landed in the capture zone during the increase of the global coverage from θ_0 at the nucleation of the island, to the actual value θ. For 3D growth, this has to equal $f \times a^p$, where a is the actual island area. The prefactor f and exponent p both depend on the exact geometrical shape. Two-dimensional growth would, e.g., result in $p = 1$, and spherical growth in $p = \frac{3}{2}$. In Fig. 5 the best fit (dashed lines) represent $p = \frac{3}{2}$, from which we conclude that the island grows in three dimensions.

Figure 5 shows some other interesting features. First of all the island denoted by • hardly grows with time. Its size remains constant at a projected area of about 1 μm^2. The island denoted by △ nucleated quite early, then stopped expanding for quite some time and continued its growth at a global coverage of about 25 ML. Its further growth follows the functional dependence given above. We conclude from the behavior of the growth rates, that the local environment plays an important role.

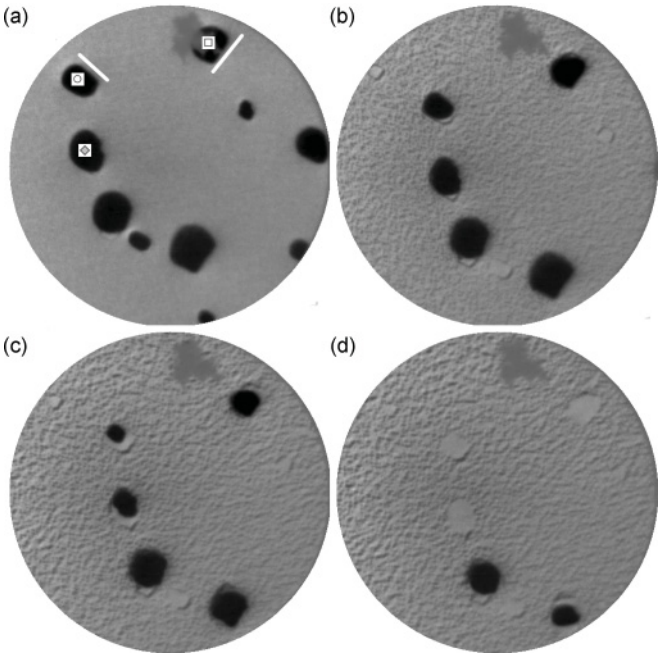

FIG. 6. (a) LEEM images of hcp-like Cu islands surrounded by a single $p(1 \times 1)$ Cu layer at a coverage of $\theta = 46.2$ ML. [(b)–(d)] At a temperature of 950 K the islands start decaying, leaving a footprint within a changed surrounding. Temperatures are 1000 K (b), 1015 K [(c),(d)]. The time elapsed between images (c) and (d) is about 100 s. All images have FoV = 10 μm and electron energy 8.0 eV. In the end situation also the persisting islands [bottom part of (d)] disappear leaving the already partly visible footprints.

VI. Cu ISLAND DECAY

Increasing the temperature to about 1000 K leads to the decay of the hcp-like Cu structures, as is shown in Figs. 6(a)–6(d). The island fractional area, dark features in Fig. 6, decreases until the islands have completely disappeared. All islands disappear and leave a footprint, which is discussed further below.

Figure 7(a) shows in detail how the decay of the projected areas evolves in time at a constant temperature of 1015 K for the islands marked with □, ○, and ◇ in Fig. 6(a) and contains information on the process, which is responsible for the decay of the Cu islands. According to the classical continuum theory in its general form[20] one can relate the decay time τ to the projected area A through $A = C \times \tau^\gamma$, where $\tau = t_f - t$, with t the actual time, t_f representing the time at which the considered island has disappeared completely, and C a detachment-related rate constant. The value of the exponent γ is characteristic for the responsible mass transport mechanism: e.g., $\gamma = \frac{2}{3}$ was demonstrated to apply for a single-layer-high Ag adatom island on Ag(111) (Ref. 21) with diffusion-limited kinetics similar to Ostwald ripening, while, e.g., $\gamma = 1$ would represent a situation in which a 2D island decays via a detachment-limited process. Detachment-limited decay of a hemisphere through the contact line followed by desorption into vacuum would lead to $\gamma = \frac{2}{3}$. Unfortunately,

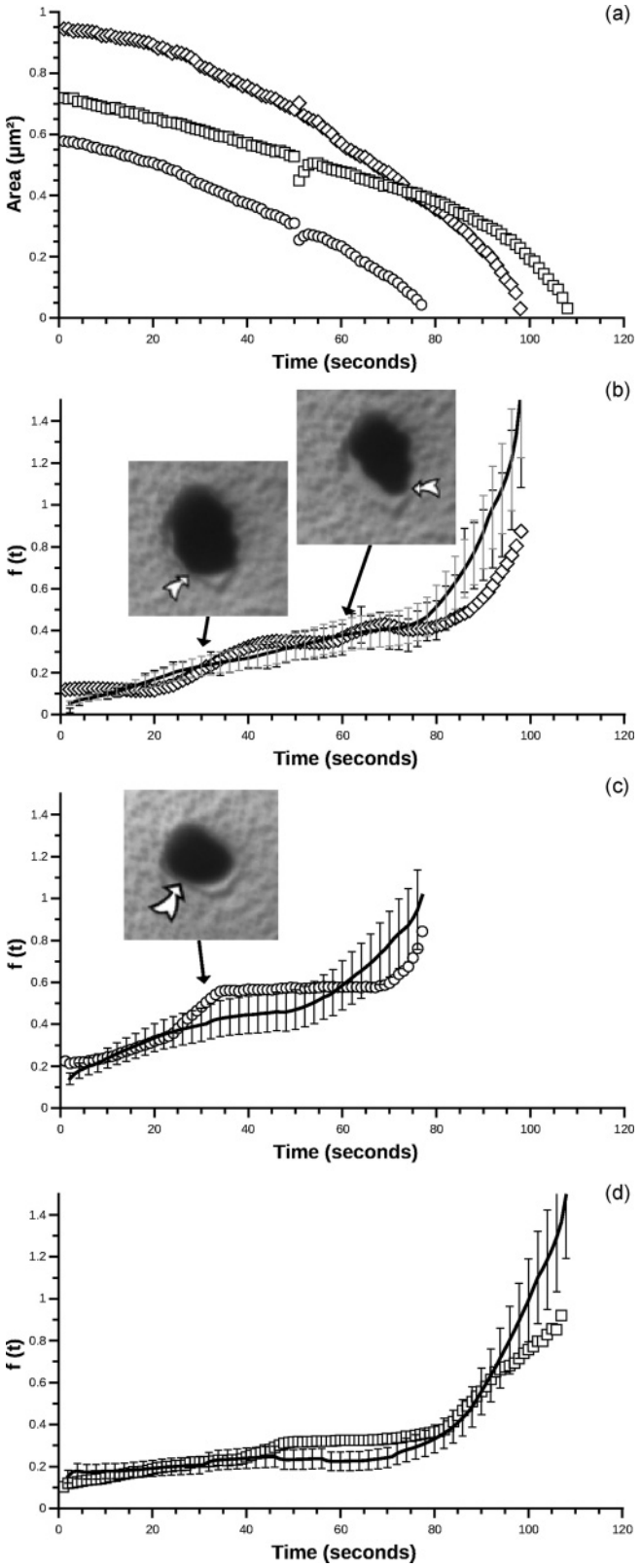

FIG. 7. (a) Island area versus time for the three islands marked in Fig. 6(a). (b)–(d) show the measured $f(t)$ for these three islands together with a derived value $f(t) = \sqrt{A/\pi} \times \frac{\delta r}{C}$ (black line) with a constant error bar of 20%. Examples of pinning that lead to variations in $f(t)$ are shown in the inset LEEM images in (b) and (c).

log-log plots of the data shown in Fig. 7(a) do not result in a clear conclusion with respect to the values of γ. A power-law fit to the decay curve for the island area denoted by □ is reasonable with an exponent 0.62, i.e., close to $\frac{2}{3}$. A worse, but still quite reasonable fit is obtained for the island denoted by ◇ for which the corresponding exponent would be 0.72. For the island referred to by ○ the result is even worse. The first part could be described with $\gamma = 0.58$, while the final part is close to $\gamma = 1.1$ and completely different values for C. In fact all three fits overestimate the initial decay rate, while the final rate is underestimated and all fits yield substantial different values for C. In conclusion, we find no unique scaling behavior in the decay characteristics. The probably most obvious failure of the power-law approach to identify the desorption process is provided by the fact that the decay curves for different islands even cross [see Fig. 7(a)].

In order to arrive at a clearer picture we carefully examined 108 frames of the decaying islands shown in Fig. 6. As is clear already from comparison of Fig. 6, parts of the circumference of the decaying islands make contact with the wetting layer, which was initially surrounding them. Initially only a small fraction of the boundary of the decaying island makes contact with the evolving footprint. Even quite close to their complete disappearance, part of the boundary of the 3D Cu islands is in contact with the wetting layer. The basic explanation is now shaped: we assume that detachment-limited decay, via the contact line with the footprint, is responsible for the temporal evolution of the Cu islands during decay.

Figures 7(b)–7(d) show the experimentally measured fraction, $f(t)$, of the total contact line that makes direct contact with the footprint for the islands marked with □, ○, and ◇ in Fig. 6(a). In all three cases we obtain a low value at $t = 0$ which strongly increases with decreasing size of the Cu islands (increasing t) near their complete disappearance. Also shown in Figs. 7(b)–7(d) as a black line is a derived "fraction" $f(t)$, derived directly from the decay curves in Fig. 7(a) using the relation $f(t) = \sqrt{A/\pi} \times \frac{\delta r}{C}$, where δr is the discrete radial decay rate, assuming detachment-limited decay via this active fraction $f(t)$ of the total contact line of a hemispherical Cu island. The detachment-related constant C for the three islands as introduced above are now all within a factor of 2. The error bar is now taken to be constant and 20% [shown in Fig. 7(a)] in view of the uncertainties and smoothening for calculating $f(t)$. In other words, all rate variations are put into $f(t)$ assuming detachment-limited decay of a 3D hemisphere.

In view of the shape assumptions, the overall correspondence between the directly measured fraction $f(t)$ and the derived one is striking: all three sets start at an initially quite low value, which gradually increases until they rise strongly near complete disappearance of the islands. The slight deviations observed near complete disappearance of each individual island are considered insignificant due to deviations from the circular shape of the contact line. Moreover, it should be noted that an exact determination of island sizes is somewhat uncertain due to inherent field distortions for 3D objects or objects with different work functions in LEEM, which becomes significant especially for small islands due to the finite pixel size. Even the deviation between the experimental and calculated $f(t)$ for $t = 30$ s and $t = 60$ s in Fig. 7(c) marked by ◇ can now be well understood. An

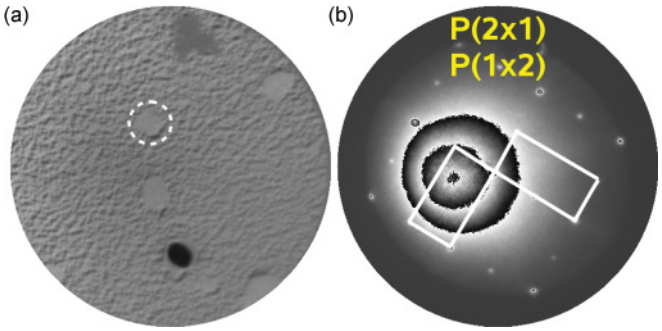

FIG. 8. (Color online) (a) LEEM image of the surface after decay of the hcp-like Cu structures. FoV = 10 μm, electron energy 8.0 eV, and $T = 1000$ K. (b) The footprints show $p(2 \times 1)$ ordering in the μLEED image taken at the dashed circle position in (a). Electron energy 31.0 eV and $T = 1000$ K.

inspection of the movie[24] revealed pinning of the contact line with the growing (decaying) footprint (island). This gives rise to an even smaller curvature of the contact line and, consequently, reduced detachment rates from this part. Depinning occurs in both cases ~10 s later. From this we can conclude that the decay of the Cu islands occurs through a detachment-limited process at the contact line between the Cu island and the evolving footprint, followed by fast desorption of the Cu adatoms.

VII. WETTING LAYER DESORPTION

As mentioned above, when the decay of the hcp-like Cu islands is completed, the islands leave a footprint [see Figs. 6(b)–6(d) and Fig. 8(a). Characterization of this footprint by μLEED at the position indicated by the dashed circle in Fig. 8(a) shows two orthogonal orientations of $p(2 \times 1)$ ordering, shown in Fig. 8(b). Such a structure indicates a surface coverage of $\theta = 0.5$ ML.

At a temperature of about 815 K, well below the temperature where hcp-like Cu island decay sets in, the wetting layer surrounding the island shows a transition. Before this transition, the wetting layer shows $p(1 \times 1)$ ordering, as is shown in Fig. 9(a). The corresponding LEEM image shows no contrast [see Fig. 9(b)]. When the wetting layer is imaged after the transition in more detail [see Fig. 9(d)], we find that it consists of small domains that have contrast that is identical to what is found in the footprints. μLEED reveals a $p(2 \times 2)$ pattern, shown in Fig. 9(c). It is the result of the coexistence of small $p(2 \times 2)$ and $p(2 \times 1)$ domains, where the latter is the more stable one. The observed structures and corresponding temperatures are in agreement with literature where the $p(2 \times 2)$ structure is attributed to a Cu-rich surface alloy with one W atom and three Cu atoms in its unit cell.[9] We must conclude that a local variation in coverage results in a reduction of the Cu coverage through thermal desorption from $\theta = 1$ ML, via $\theta = 0.75$ ML [$p(2 \times 2)$] to $\theta = 0.5$ ML [$p(2 \times 1)$]. Temperature programmed desorption (TPD) measurements show thermal desorption at 1100 K for coverages $\theta < 1$ ML.[8,9] Note that the time scales used are radically different. Here we deal with a typical time scale of 900 s, while the heating rate in the TPD literature data vary between 4 and 130 K/s. The surface alloying that is revealed by the appearance of the $p(2 \times 2)$ pattern is confirmed by a

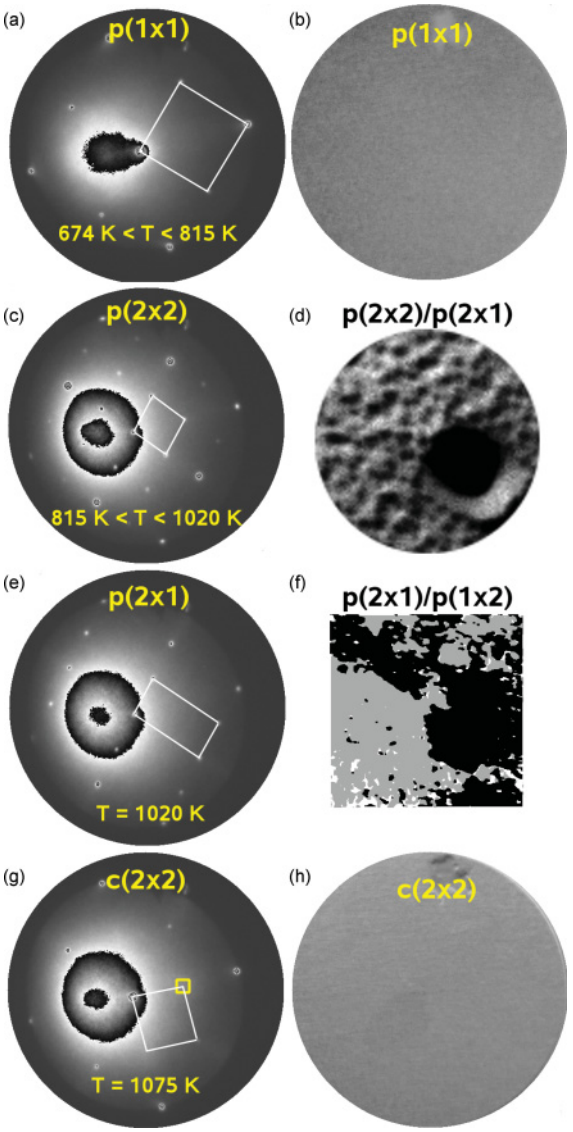

FIG. 9. (Color online) (a) μLEED image taken at 31.0 eV and (b) LEEM image for the $p(1 \times 1)$ Cu layer found for 674 K< T <815 K, FoV = 10 μm; electron energy is 8.0 eV. (c) μLEED image for the $p(2 \times 2)$ structure and a $p(2 \times 1)$ structure found for 815 K< T < 1020 K; electron energy is 31.0 eV. (d) The corresponding LEEM image shows small domains of $p(2 \times 2)$ and $p(2 \times 1)$ surface alloys, FoV = 2 μm, and electron energy is 8.0 eV. The large dark area near the center is a Cu hcp island. The numerous smaller black spots are assigned to the Cu-rich $p(2 \times 2)$ domains. (e) μLEED image for a large $p(2 \times 1)$ domain created at $T = 1020$ K; electron energy is 31.0 eV. (f) A composite image constructed of dark-field images from the $(\frac{1}{2},0)$ and $(0,\frac{1}{2})$ diffraction spots, revealing the domains of the $p(2 \times 1)$ and $p(1 \times 2)$ structures. The light gray areas have been obtained from using the $(\frac{1}{2},0)$ spots, while the dark areas have been obtained with the $(0,\frac{1}{2})$ spot. For the latter the contrast of the high-intensity areas has been reversed into black. A few smaller white areas were observed too, where the (2×1) and (1×2) intensities are equal, possibly related to $c(2 \times 2)$ domains. Image size is 6.8×6.8 μm^2. (g) μLEED image of the diffuse $c(2 \times 2)$ surface alloy diffraction pattern at $T = 1075$ K; electron energy is 31.0 eV. The integrated spot intensity (see Fig. 10), is measured in the area marked by the small yellow (white) square. (h) The corresponding LEEM image, FoV = 10 μm; electron energy is 8.0 eV.

corresponding increase in the W(1,0) diffraction spot intensity of about 25% between 800 and 900 K. The increase results from the alloying in which more W atoms become visible in the outermost layer. Their larger atomic scattering factor, in comparison to Cu, gives rise to enhanced intensity in the integral order spots.

For temperatures above 1000 K we find that the small and dark Cu-rich $p(2 \times 2)$ patches disappear and we lose contrast on the surface in our bright field images. This is indicative of the desorption of Cu from the ordered Cu-rich patches. We are left with the $p(2 \times 1)$ patches and the total coverage decreases to a value of $\theta = 0.5$ ML, shown in Fig. 9(e). By measuring the corresponding dark-field images on the $(0,\frac{1}{2})$ and $(\frac{1}{2},0)$ spots we are able to image both rotations of the $p(2 \times 1)$ domains, clearly segregated. Combining these images results in the composite image shown in Fig. 9(f).

Upon reaching a coverage of $\theta = 0.5$ ML, we anticipated to observe $c(2 \times 2)$ ordering, as known from literature.[9] This structure has been reported to be stable up to thermal desorption at 1100 K.[9] However, the different route of formation via a Cu-rich phase leads to the $p(2 \times 1)$ domain. Only at $T = 1075$ K do we find a diffuse $c(2 \times 2)$ diffraction pattern, as is shown in Fig. 9(g), where the corresponding LEEM image in Fig. 9(h) reveals no contrast. The broad $(\frac{1}{2},\frac{1}{2})$ diffraction spots indicate small $c(2 \times 2)$ and probably defect-rich surface alloy structures.[9]

This remarkable structural ordering toward complete thermal desorption was followed *in situ* with LEED and illustrated in Fig. 10. The spot intensities for the $(\frac{1}{2},\frac{1}{2})$, $(\frac{1}{2},0)$, and $(0,\frac{1}{2})$ spot during heating of the sample at a linear rate of 2.64 K/s is depicted. The intensity in the $(\frac{1}{2},\frac{1}{2})$ diffraction spot corresponds to both $p(2 \times 2)$ and $c(2 \times 2)$ structures, where the intensity in the $(\frac{1}{2},0)$ spot corresponds to both $p(2 \times 2)$ and $p(2 \times 1)$ ordering. Unlike earlier reports in literature,[9] the $(\frac{1}{2},0)$ diffraction spot of the $p(2 \times 2)$ structure does not show attenuation before the $(\frac{1}{2},\frac{1}{2})$ spot does. At $T = 985$ K the $(\frac{1}{2},\frac{1}{2})$ spot intensity shows a maximum, revealing the onset of the transition of $p(2 \times 2)$ domains into $p(2 \times 1)$ domains by thermal desorption. The $p(2 \times 1)$ shows its maximum diffraction intensity at $T = 1010$ K as a sharp spot where the $(0,\frac{1}{2})$ spot intensity does not, since no intensity of the $p(2 \times 2)$ domains contributes to the $(\frac{1}{2},0)$ diffraction spot at this temperature. At a temperature of 1075 K, we find broad diffuse intensity at the $(\frac{1}{2},\frac{1}{2})$ diffraction spot, corresponding to small $c(2 \times 2)$ domains. From these findings we suggest that at a coverage of $\theta = 0.5$ ML, both the $p(2 \times 1)$ and $c(2 \times 2)$ surface alloy structures are stable, where the first occurs as the result of desorption from a Cu-rich coverage of $\theta > 0.5$ ML. Apparently the energy barrier for the transition from the $p(2 \times 1)$ structure into the more favorable $c(2 \times 2)$ structure is almost similar to the desorption energy. The energy barrier from the (meta)stable $p(2 \times 1)$ structure toward the more stable $c(2 \times 2)$ surface alloy can only be overcome at temperatures where desorption occurs simultaneously. Probably, desorption-induced vacancies, which are known to enhance diffusion,[22,23] are necessary to lower the effective energy barrier, which has to be overcome to form the $c(2 \times 2)$ phase. Therefore, a diminishing coverage is left to create small $c(2 \times 2)$ domains for $T > 1020$ K, resulting in the corresponding broad diffraction spots. For temperatures over 1150 K, no signature of any Cu surface structure was measured.

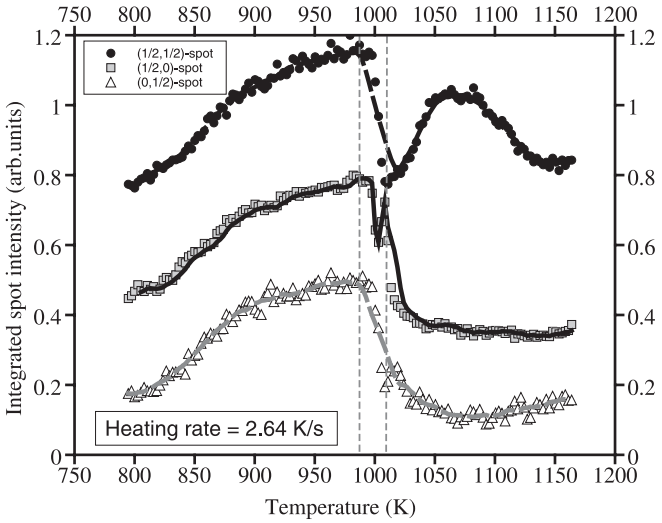

FIG. 10. The integrated spot intensities for the $(\frac{1}{2},\frac{1}{2})$, $(\frac{1}{2},0)$ and $(0,\frac{1}{2})$ diffraction spots (offset) as a function of temperature. The lines at T = 985 K and T = 1010 K show the maximum integrated intensity for the $(\frac{1}{2},\frac{1}{2})$, $(\frac{1}{2},0)$ and $(0,\frac{1}{2})$ LEED spots measured with a 1.4 μm aperture. The aperture size is smaller than the typical domain size, see Fig. 8(f), hence only one of the two possible orientations is visible.

VIII. CONCLUSIONS

The deposition of several tens of monolayers of Cu on W(100) at 674 K leads to the evolution of hut-shaped Cu crystallites with steep facets with angles of about 54°. The structure of the crystallites is consistent with a hexagonal close-packed structure with the $(11\bar{2}0)$ plane parallel to W(100). The boundary of the Cu crystallites intersects the close-packed W(100) azimuth at 11.3°, which corresponds to the $[\bar{1}50]$ azimuth. This can be explained by a cancellation of shear stress exerted by the hcp Cu crystallites by introducing stacking faults in the $(1\bar{1}00)$ layers at a mean distance of four close-packed layers.

The pseudomorphic Cu wetting layer transforms to a surface alloy with Cu-rich $p(2 \times 2)$ and $p(2 \times 1)$ domains at 815 K. The hut clusters desorb at 950 K. They leave behind footprints with $p(2 \times 1)$ ordering surrounded by the bidomain wetting layer. The desorption proceeds via detachment-limited decay at the contact line between the Cu islands and the evolving footprint. Upon further heating the entire surface is covered by the $p(2 \times 1)$ surface alloy, and only just before complete desorption of Cu from the surface layer small $c(2 \times 2)$ domains develop. This demonstrates that the latter structure is thermodynamically favored.

ACKNOWLEDGMENTS

This work is part of the research programme of the Foundation for Fundamental Research on Matter (FOM), which is financially supported by the Netherlands Organization for Scientific Research (NWO).

[1]Y.-W. Mo, D. E. Savage, B. S. Swartzentruber, and M. G. Lagally, Phys. Rev. Lett. **65**, 1020 (1990).
[2]A. J. Steinfort, P. M. L. O. Scholte, A. Ettema, F. Tuinstra, M. Nielsen, E. Landemark, D.-M. Smilgies, R. Feidenhans'l, G. Falkenberg, L. Seehofer, and R. L. Johnson, Phys. Rev. Lett. **77**, 2009 (1996).
[3]A. T. Paxton, M. Methfessel, and H. M. Polatoglou, Phys. Rev. B **41**, 8127 (1990).
[4]H. Wormeester, E. Hüger, and E. Bauer, Phys. Rev. Lett. **77**, 1540 (1996).
[5]H. Wormeester, E. Hüger, and E. Bauer, Phys. Rev. Lett. **81**, 854 (1998).
[6]W. Wulfhekel, T. Gutjahr-Löser, F. Zavaliche, D. Sander, and J. Kirschner, Phys. Rev. B **64**, 144422 (2001).
[7]H. Wormeester, M. Kiene, E. Huger, and E. Bauer, Surf. Sci. **377**, 988 (1997).
[8]E. Bauer, H. Poppa, G. Todd, and F. Bonczek, J. Appl. Phys. **45**, 5164 (1974).
[9]G. Attard and D. King, Surf. Sci. **188**, 589 (1987).
[10]P. Hu, A. Wander, L. de la Garza, M. Bessent, and D. King, Surf. Sci. **286**, L542 (1993).
[11]M. Harrison, D. Woodruff, and J. Robinson, Surf. Sci. **572**, 309 (2004).
[12]K. Zakeri, T. Peixoto, Y. Zhang, J. Prokop, and J. Kirschner, Surf. Sci. **604**, L1 (2010).
[13]D. S. Choi and D. H. Kim, Mod. Phys. Lett. B **23**, 835 (2009).
[14]F. Buatier de Mongeot, W. Zhu, A. Molle, R. Buzio, C. Boragno, U. Valbusa, E. G. Wang, and Z. Zhang, Phys. Rev. Lett. **91**, 016102 (2003).
[15]S. van Dijken, L. C. Jorritsma, and B. Poelsema, Phys. Rev. B **61**, 14047 (2000).
[16]Z. Tang, M. Hasegawa, Y. Nagai, and M. Saito, Phys. Rev. B **65**, 195108 (2002).
[17]Z. Q. Wang, S. H. Lu, Y. S. Li, F. Jona, and P. M. Marcus, Phys. Rev. B **35**, 9322 (1987).
[18]H. Li, D. Tian, J. Quinn, Y. S. Li, F. Jona, and P. M. Marcus, Phys. Rev. B **43**, 6342 (1991).
[19]L. Bruce and H. Jaeger, Philos. Mag. A **37**, 337 (1978).
[20]M. Zinke-Allmang, L. C. Feldman, and M. H. Grabow, Surf. Sci. Rep. **16**, 377 (1992).
[21]K. Morgenstern, G. Rosenfeld, and G. Comsa, Phys. Rev. Lett. **76**, 2113 (1996).
[22]R. van Gastel, E. Somfai, S. B. van Albada, W. van Saarloos, and J. W. M. Frenken, Phys. Rev. Lett. **86**, 1562 (2001).
[23]E. Somfai, R. van Gastel, S. B. van Albada, J. W. M. Frenken, and W. van Saarloos, Surf. Sci. **521**, 26 (2002).
[24]See also Supplemental Material at http://link.aps.org/supplemental/10.1103/PhysRevB.85.125417 for a LEEM movie showing the decay of hcp-Cu islands accompanying the single frames in Fig. 6 as well as the insets in Fig. 7.